Transcriptome-wide identification of 5-methylcytosine by deaminase and reader protein-assisted sequencing

Jiale Zhou[1#], Ding Zhao[1#], Jinze Li[2#], Deqiang Kong[1], Xiangrui Li[2], Renquan Zhang[2], Yuru Liang[2], Xun Gao[2], Yuqiang Qian[2], Di Wang[2], Jiahui Chen[2], Liangxue Lai [1,3,4*], Yang Han[2*], Zhanjun Li [2*]

# These authors contributed equally: Jiale Zhou, Ding Zhao, Jinze Li.

[1]Key Laboratory of Zoonosis Research, Ministry of Education, College of Veterinary Medicine, Jilin University, Changchun, 130062, China

[2]Laboratory Animal Center, College of Animal Science, Jilin University, Changchun, 130062, China

[3]Guangzhou Regenerative Medicine and Health Guang Dong Laboratory (GRMH-GDL), Guangzhou, 510530, China

[4]Institute for Stem Cell and Regeneration, Chinese Academy of Sciences, Beijing, 510005, China

* To whom correspondence should be addressed:

Tel: (86)431-87836176; Fax: (86)431-87980131;

*e-mail:

hanyang8584@jlu.edu.cn (Yang Han); lizj_1998@jlu.edu.cn (Zhanjun Li); lai_liangxue@gibh.ac.cn (Liangxue lai).

Abstract

5-Methylcytosine (m^5C) is one of the major post-transcriptional modifications in mRNA and is highly involved in the pathogenesis of various diseases. However, the capacity of existing assays for accurately and comprehensively transcriptome-wide m^5C mapping still needs improvement. Here, we develop a detection method named DRAM (deaminase and reader protein assisted RNA methylation analysis), in which deaminases (APOBEC1 and TadA-8e) are fused with m^5C reader proteins (ALYREF and YBX1) to identify the m^5C sites through deamination events neighboring the methylation sites. This antibody-free and bisulfite-free approach provides transcriptome-wide editing regions which are highly overlapped with the publicly available BS-seq datasets and allows for a more stable and comprehensive identification of the m^5C loci. In addition, DRAM system even supports ultra-low input RNA (10ng) and monitor the dynamic accumulation of cellular m^5C. We anticipate that the DRAM system could pave the way for uncovering further biological functions of m^5C modifications.

Keywords: RNA, 5-Methylcytosine, deaminase, m^5C reader

Introduction

Epigenetics refers to stable inheritance without changing the basic sequence of DNA, involving various forms such as DNA methylation, histone modification and RNA modification. In recent years, RNA sequencing technology has boosted research on RNA epigenetics. More than 170 RNA modifications have been identified, mainly including m^6A, m^5C, m^1A, m^7G and others [1,2]. Notably, RNA m^5C methylation represents a crucial post-transcriptional modification observed across different RNA types, such as tRNA, mRNA, rRNA, vault RNA, microRNA, long non-coding RNA and enhancer RNA[3-8]. Numerous studies have revealed multiple molecular functions of m^5C in numerous key stages of RNA metabolism, such as mRNA stability, translation, nuclear export[5,9-13]. And the dynamic alterations of m^5C play integral roles in many physiological and pathological processes, such as early embryonic development[14], neurodevelopmental disorder[15,16] and multifarious tumorigenesis and migration[17-20]. Moreover, this modification significantly contributes to the regulation of gene expression[5,9-13,17]. Therefore, the detection of m^5C sites appears to be essential for understanding its underlying effects on cellular function and disease states.

With the recent advances in sequencing techniques, several high-throughput assays have been developed for qualitative or quantitative analysis of m^5C. To date, bisulfite-sequencing (BS-seq) has been proved to be the gold standard method for RNA m^5C methylation analysis[5,21,22]. This approach chemically deaminates unmethylated cytosine to uracil, while kept methylated cytosine unchanged. The m^5C methylation sites can be identified by subsequent library construction and sequencing. However, bisulfite treatment of BS-seq is extremely detrimental to RNA, thus resulting in unstable detection of m^5C in low abundance RNA or highly structured RNA, which directly affects the confidence of results[23,24]. Another major type of global m^5C analysis depends on antibody-assisted immunoprecipitation of m^5C methylated RNAs, such as m^5C-RIP-seq[25-27], AZA-IP-seq[28] or miCLIP-seq[7]. These methods are unable to recognize methylation on mRNAs with low abundance and secondary structure. Moreover, these methods are highly dependent on antibody specificity, which usually lead to unspecific binding of RNA and low amount of m^5C-modified regions. Moreover, TAWO-seq, originally developed for the identification of hm^5C, is also capable for m^5C analysis, but it highly depends on the oxidation efficiency of perovskite, which usually cause false positives and unstable conversion [29,30]. Furthermore, the emerging third generation sequencing, such as Nanopore-seq, can directly map m^5C by tracking the characteristic changes of bases, but it still faces challenges of a high error rate[31-33].These together largely hampers its wide application on transcriptome profiling of m^5C (Supplementary Table 1). Hence, there is an urgent need for a simple, efficient, sensitive, and antibody-independent method for global m^5C detection.

The RNA-binding protein ALYREF is the initially recognized nuclear m^5C reader that binds directly to m^5C sites in mRNA and play key roles in promoting mRNA nuclear export or tumor progression[5]. Another well-known m^5C reader, YBX1, can also recognize m^5C-modified mRNA through its cold-shock domain, and participates in a variety of RNA-dependent events such as mRNA packaging, mRNA stabilization and translational regulation[9,18]. YBX1 can preferentially recognize mRNAs with m^5C modifications via key amino acids W65-N70 (WFNVRN)[18], while K171 is essential for the specific binding of ALYREF to m^5C sites [5].

Nucleic acid deaminases, primarily categorized as cytosine deaminases and adenine

deaminases, are zinc-dependent enzymes which facilitate the deamination of cytosine or adenine within DNA or RNA substrates[34]. APOBEC1, an evolutionarily conserved family member of APOBEC proteins, can specifically catalyze the deamination of cytosine in single stranded RNA (ssRNA) or DNA (ssDNA) to uracil[35-37]. TadA8e is an adenine deaminase optimized through re-engineering of TadA and it induces conversion of adenine to inosine (eventually read as guanine by transcriptases) in ssRNA or ssDNA[38,39]. APOBEC1 and TadA8e, with their prominent deamination efficiency, have been employed for the development of precise and efficient base editors such as CBE and ABE8e, which find widespread application in studies related to genome editing[37,38].

Here we aim to establish a deaminase and m^5C reader-assisted RNA methylation sequencing approach (DRAM-seq), which identifies the m^5C sites through reader-mediated recognitions and deaminase-mediated point mutations neighboring the m^5C methylation sites. This bisulfite-free and antibody-free method is anticipated to provide more comprehensive and cost-effective transcriptome-wide detection of m^5C methylation, which may better assist on exploring its further regulatory mechanisms.

Results

Development of DRAM system for m^5C detection

Our sequencing platform is inspired by the concept of the m^6A DART-seq assay, in which C near the m^6A site is converted into U without affecting sequences near non-m6A sites[40]. Therefore, we hypothesized that, by utilizing the targeted binding of m^5C readers, deaminase can be recruited to achieve deamination of cytosine or adenine in the vicinity of the m^5C sites on single-stranded RNA, thereby facilitating the detection of the m^5C site. This approach was named DRAM (deaminase and m^5C reader-assisted RNA methylation sequencing). As RNA-binding proteins, ALYREF and YBX1 also could bind to RNAs without m^5C modification[5,18]. In order to exclude the false-positive detection of DRAM due to the non-m^5C specific binding of ALYREF and YBX1, knockout of W65-N70 (WFNVRN) amino acids in YBX1and K171A mutation in ALYREF were introduced seperately, resulting in the $DRAM^{mut}$ system (Fig. S1, Supporting Information). To confirm the recognition of m^5C site by DRAM system, DRAM, $DRAM^{mut}$ and Deaminase system were transfected into the human HEK293T cells, respectively. Finally the m^5C regions were identified by detecting the C-to-U/A-to-G transition, which only occur in the presence of the DRAM system, but not in the presence of the corresponding $DRAM^{mut}$ and Deaminase system (Fig. 1A).

Previous studies have indicated that there is no uniform intrinsic signature motif sequence that can characterize all m^5C sites[5,26,41,42]. To comprehensively detect the m^5C loci, the readers of m^5C (ALYREF and YBX1) were separately fused to the C-terminus of the deaminases (APOBEC1 and TadA-8e), namely DRAM-ABE and DRAM-CBE system (Fig.1B).

DRAM detection system is assayed in an m^5C-dependent form

To confirm the recognition of m5C site by DRAM system, DRAM, $DRAM^{mut}$ and Deaminase were transfected into the human HEK293T cells, respectively. Two previously reported m^5C sites in RPSA and AP5Z1 were selected for the analysis [5,21], and their methylation status were verified

by bisulfite sequencing PCR. The deep sequencing results showed that the deamination rates of RPSA and SZRD1 were 75.5% and 27.25%, respectively. (Fig.2A and B). Sanger sequencing following RT-PCR was then performed to determine the editing of neighbouring m^5C sites by DRAM system in these two mRNA. Notably, adenine close to the m^5C site in RPSA mRNA was mutated into guanine, resulting in an A-to-G editing rate of 14.7% by DRAM-ABE, whereas this was rarely observed with TadA-8e or $DRAM^{mut}$-ABE (Fig.2C). DRAM-CBE induced C to U editing in the vicinity of the m^5C site in AP5Z1 mRNA, with 13.6% C-to-U editing, while this effect was significantly reduced with APOBEC1 or $DRAM^{mut}$-CBE (Fig.2D). Taken together, the fusion of m^5C reader and deaminase can effectively and selectively deaminate cytosine/adenine in the vicinity of the m^5C sites.

NSUN2[43] and NSUN6[44], two family members of NOL1/NSUN protein, were both identified as m^5C methyltransferase of mRNA[45]. To verify that the detection of DRAM occurs in the presence of m^5C, we individually depleted NSUN2 and NSUN6 in HEK293T cells and performed DRAM transfection. The knockout efficiency has been confirmed by western blotting (Fig.2E, 2F and Fig. S2, Supporting Information). It has been previously demonstrated that m^5C methylation of AP5Z1 and RPSA are catalyzed by NSUN2 and NSUN6, respectively[21,46]. In line with this, sanger sequencing following RT-PCT showed a significant reduction in C-to-U or A-to-G mutations near the m^5C sites in methyltransferase-deficient cells compared with WT cells (Fig. 2G and H). Overall, these findings suggest that the DRAM detection system is assayed in an m^5C-dependent form.

DRAM enables transcriptome-wide analysis of m^5C methylation

Subsequently, we performed RNA-seq after DRAM transfection to enable a transcriptome-wide detection of m^5C. To serve as positive controls, two previously published BS-seq datasets were also integrated[5,21]. Mutations were detected near the m^5C site in RPSA as A-to-G by DRAM-ABE (Fig.3A), and DRAM-CBE detected the presence of C-to-U mutations near the AP5Z1 m^5C site (Fig.3B). However, the $DRAM^{mut}$ and Deaminase systems induced few effective mutations close to these sites. Examination of multiple reported high-confidence RNA m^5C sites showed that DRAM-seq editing events were also enriched in the vicinity of the BS-seq sites (Fig.3A, 3B and Fig. S3, Supporting Information). Comparison of three biological replicates revealed a strong reproducibility of A-to-G/C-to-U mutations in HEK293T cells expressing DRAM-ABE and DRAM-CBE (Fig. S4, Supporting Information). This finding suggests that DRAM selectively targets specific RNAs for editing, exhibiting a high degree of consistency across samples.

DRAM-seq analysis further confirmed that DRAM was detected in an m^5C-dependent manner, with minimal mutations in AP5Z1 and RPSA mRNAs in methyltransferase knockout cells compared to wild-type cells (Fig. 3C, D). Moreover, the knockout cells exhibited overall rare DRAM-seq editing events close to m^5C sites in other mRNAs (Fig. S5, Supporting Information).

To obtain information on a set of high-confidence DRAM-seq data, we filtered the list of sites transfected with deaminase alone and screened the sequencing results with methyltransferase depleted, pooled editing events occurring in at least 10% of reads across multiple samples to obtain a set of high-confidence editing sites (Supplementary Table 2), and integrated genes with editing sites occurring in DRAM-ABE and DRAM-CBE (Supplementary Table 3).

Previous studies have indicated that m^5C sites are predominantly distributed in the coding

sequences (CDS) and notably enriched near the initiation codon[5,25,26,47-49]. To further delineate the characteristics of the DRAM-seq data, we compared the distribution of DRAM-seq editing sites within the gene structure, specifically examining their occurrences in the 5'untranslated region (5'UTR), 3' untranslated region (3'UTR), CDS and ncRNA. Our analysis revealed that DRAM-seq editing events in cells expressing DRAM-ABE and DRAM-CBE were primarily located in the CDS and 3'UTR, indicating a non-random distribution of m^5C (Fig.3E, Fig. S6A and 6B, Supporting Information). Moreover, plotting the distribution of DRAM-seq editing sites in mRNA segments (5'UTR, CDS, and 3'UTR) highlighted a significant enrichment near the initiation codon (Fig.3F). In contrast, cells expressing the deaminase exhibited a distinct distribution pattern of editing sites, characterized by a prevalence throughout the 5'UTR. This finding reaffirms that the specific editing pattern observed in DRAM-seq across the transcriptome depends on its capacity to bind m^5C (Fig.3F).

Comparative analysis of the DRAM-seq editing sites with the previously published BS-seq m^5C sites indicated that the likelihood of editing was notably higher in closer proximity to the m^5C sites (Fig.3G). Furthermore, the editing window of DRAM exhibited enrichment approximately 20bp before and after the m^5C site (Fig.3G). Investigation into the sequences surrounding the editing window revealed that AC motifs were the most significantly enriched in DRAM-CBE, whereas (U/C) A motifs were most notably enriched in DRAM-ABE. In contrast, the APOBEC1 and TadA-8e samples displayed no significantly enriched motifs, with mutations being more randomly orientated (Fig.3H, I).

DRAM-seq provides stable and comprehensive identification of m^5C loci

Subsequently, we assessed the capacity of DRAM-seq to detect m^5C on a transcriptome-wide scale, comparing its performance to BS-seq that have been previously reported with great authority. Although both previous studies employed bisulfite treatment, the resulting data obtained significantly discrepancies due to variations in their treatment and analysis methodologies. Our results indicated that DRAM-seq identified the presence of m^5C modifications covering 82.5% of the genes detected by Yang et al.[5] and 95.5% of the genes detected by Zhang et al.[21] (Fig.4A and C). Remarkably, certain pivotal regulators with diverse biological functions, such as ATG16L1(coordinats autophagy pathway)[50] and ARHGEF25 (plays an important role in actin cytoskeleton reorganisation)[51], were identified by Zhang et al. and DRAM-seq, but not by Yang et al. (Fig.4B). Conversely, FANCD2 (Maintains chromosome stability)[52] and RPL15(components of the large ribosomal subunit)[53,54], were discovered by Yang et al. and DRAM-seq, but not by Zhang et al. (Fig.4D). Hence, DRAM-seq appears to offer a more stable and comprehensive identification of the m^5C loci.

To provide functional insights into m^5C RNA-modified genes in HEK293T cells, we conducted Gene Ontology (GO) and Kyoto Encyclopedia of Genes and Genomes (KEGG) analyses. These results highlighted the involvement of these genes in the regulation of diverse key biological processes, such as cell division, cell cycle, mRNA splicing, protein processing in the endoplasmic reticulum, nucleocytoplasmic transport, translation, DNA repair and others (Fig.4E, 4F, Fig S6C and S6D, Supporting Information).

DRAM monitors m^5C dynamics in cellular RNA

Next, we aim to determine whether changes in m^5C can be detected in real-time by DRAM.

Previous studies have established that oxidative stress induced by 200 μM sodium arsenite ($NaAsO_2$) treatment inhibited the expression of NSUN2 and NSUN6, resulting in a gradual decrease in m^5C methylation[55,56]. As cells exposed to $NaAsO_2$ typically exhibited slowed cell cycle progression and $NaAsO_2$ induce apoptosis, we performed a low concentration screen[57,58]. After gradient treatment of $NaAsO_2$ (50μM, 100μM, 150μM, and 200μM, separately) in cells, 200μM group was identified as the optimal concentration, leading to highly significant decreases of NSUN2 and NSUN6 expression (Fig.5A). Subsequently, HEK293T cells expressing DRAM with $NaAsO_2$ for 3 hours revealed a decreasing trend in the mRNA expression of NSUN2 and NSUN6 (Fig.5B).

Sanger sequencing results showed that induction of the DRAM system after $NaAsO_2$ treatment resulted in a highly significant reduction of A-to-G/C-to-U mutations on both RPSA and AP5Z1 mRNAs compared to cells without $NaAsO_2$ treatment (Fig.5C and D). To confirm this analysis, we employed bisulfite sequencing PCR to verify that m^5C levels in selected mRNAs displayed a decreasing trend after $NaAsO_2$ treatment (Fig.5E and F). Thus, the DRAM effectively detects changes in m^5C, providing a valuable tool for monitoring the accumulation of m^5C in individual RNAs in response to alterations cellular conditions.

DRAM enables low-input m^5C profiling

A significant challenge in m^5C detection lies in the specificity of antibodies and the substantial amount of input RNA required for sequencing. RNA is susceptible to degradation during denaturation, sodium bisulfite treatment and desulfurization steps in the BS-seq assay[59]. Immunoprecipitation-based m^5C assays and LC-MS/MS also impose high demand for sample input[7,25,60]. Several experiments have highlighted the requirement of 100-500 ng of RNA for m^5C-RIP-seq, while BS-seq necessitates an even more demanding 500-750μg of RNA[21,25,61]. To assess the detection limits of DRAM-Sanger, we attempted to amplify two representative m^5C-containing sites in the RPSA and AP5Z1 transcripts from diluted RNA samples.

Remarkably, we successfully generated PCR products of these two mRNAs from cDNAs corresponding to 250 ng, 50 ng, and 10 ng of total RNA. Quantitative analysis by Sanger sequencing demonstrated nearly identical Sanger traces across these dilutions (Fig.5G and H). This finding underscores that the specificity of DRAM editing depended on its ability to bind m^5C, and DRAM is proficient in low-input m^5C analyses. Furthermore, cell viability was determined by CCK8 assay on HEK293T cells transfected with DRAM (Fig.5I). Importantly, there was no significant difference in the relative proliferative capacity of the cells compared to untransfected cells (NC), indicating that DRAM expression did not adversely affect cell viability (Fig.5J).

Conclusions

In summary, we developed a novel deaminase and reader protein assisted RNA m^5C methylation approach, which does not rely on antibodies or bisulfite, thus leading to unprecedently comprehensive transcriptome-wide RNA m^5C methylation profiling. We anticipated that this system could pave the way for uncovering further biological functions of m^5C modifications and facilitate the development of therapeutic interventions for associated diseases.

Discussion

In recent years, m^5C methylation modifications have received increasing attention, with multiple reports detailing the distribution of RNA m^5C methylation modifications across various species and tissues, elucidating their characteristics. Despite the relatively low abundance of m^5C, its highly dynamic changes hold significant implications for the regulation of physiological and pathological processes[5,21,44].However, due to the limitations of sequencing methods and the variability of data processing, there remains ample room for progress in the study of m^5C detection methods.

In this study, we developed site-specific, depth-sequencing-free m^5C detection method using DRAM-Sanger. This workflow relies on conventional molecular biology assays such as RT-PCR and Sanger sequencing, eliminating the need for specialized techniques and thereby simplifying the process of m^5C detection.

DRAM-seq introduce a novel strategy for transcriptome-wide m^5C detection, overcoming inherent limitations in existing methods. Notably, DRAM-seq covered 82% of the high-confidence m^5C modified genes detected by BS-seq, and identified more potential m^5C sites. This can be attribute to the avoidance of bisulfite treatment by DRAM-seq, preventing RNA damage and ensuring a more comprehensive representation of RNA samples. This feature also likely contributes to the observed stability of DRAM-seq in comparison to BS-seq. Additionally, DRAM-seq is not constrained by antibody specificity and is resistant to chemical reagent-induced damage, preserving the gene expression information captured by typical RNA-seq. Consequently, DRAM-seq uniquely provides the capability to report both transcript abundance and information related to m^5C modifications.

A prominent challenge in existing m^5C profiling methods is their reliance on substantial amounts of input RNA samples. In contrast, DRAM operates through the deamination activity of deamination activity of deaminase, preserving RNA integrity and preventing degradation. The notable advantage of DRAM lies in its capacity for low-input m^5C detection. Our analysis demonstrates that DRAM requires as low as 10ng of total RNA for m^5C detection. While DRAM is currently well-suited for detecting m^5C on a transcriptome-wide scale, the potential for future applications involving third generation sequencing could extend its utility to individual mRNAs, particularly m^5C heterogeneity on mRNA splicing variants. In addition, the DRAM system depends on the specific recognition of m^5C modifications on ssRNA by the reader protein, theoretically avoiding the false-positive effects of 5-hydroxymethylation modifications in other assays, such as BS-seq[21-23]. This potential feature could enhance the accuracy of the DRAM assay, albeit it still requires careful validation.

In our study, m^5C detection was performed following the transient transfection of the DRAM detection system into mammalian cells, which might result in a lower mutation rate at the corresponding site. Therefore, employing lentiviral-mediated transfection into cell lines of interest could potentially enhance the efficiency of m^5C detection. Further elucidation of the key amino acids directing ALYREF and YBX1's binding to m^5C methylation sites should enable more accurate and sensitive m^5C detection by DRAM-seq. Since m^5C lacks a fixed motif, DRAM has an apparent limitation in achieving single-base resolution for detecting m^5C. However, our present study proved that the measuring resolution of DRAM is around 40nt, which facilitates higher precision than that of m^5C-RIP-seq (~100nt). In the future, with the in-depth structural analysis of the m^5C current readers and the identification of new m^5C readers, we anticipated to better determine the motif of m^5C for its accurate localization. Moreover, the substitution of deaminases,

such as A3A and A3G (the family members of APOBEC), could also potentially enhance the efficiency of the DRAM detection [62-64].

Following the purification of DRAM fusion protein, achieving *in vitro* detection of RNA m^5C methylation could broaden the applicability to a more diverse range of samples. Another potential application for DRAM-seq could be the expression of drug-inducible DRAM systems *in vivo* using various animal models for m^5C analysis. These will together provide novel insights of m^5C modifications for biological and clinical research.

Materials and methods

Plasmid construction

ALYREF and YBX1 expression plasmids were purchased from MIAOLING BIOLOGY (http://www.miaolingbio.com/), and the ALYREF and YBX1 fractions were then amplified using specific primer. The ALYREF and YBX1 portions were amplified using pCMV-APOBEC1-YTH (Addgene plasmid no. 131636; https://www.addgene.org/131636/) and ABE8e (Addgene plasmid no. 138489; https://www.addgene.org/ 138489/) to amplify the deaminase portion and the essential plasmid construct proxies, and finally the fragments were recombined by the ClonExpress Ultra One Step Cloning Kit to complete the plasmid vector construction. Both $DRAM^{mut}$-ABE and $DRAM^{mut}$-CBE related vectors were obtained by introducing the corresponding key amino acid mutations using Fast Site-Directed Mutagenesis Kit (TIANGEN Biotech). The primer sequences used are listed in Supplementary Table 4.

Cell culture and plasmid transfection

HEK293T cell line (ATCC) was cultured in Dulbecco's Modified Eagle Medium (DMEM) supplemented with 10% fetal bovine serum (CLARK BIOSCIENCE) and 1% penicillin (100 U/ml)-streptomycin (100μg/ml). The cells were seeded in 12-well plates and transfected using Hieff Trans™ Liposomal Transfection Reagent (Yeasen).

NSUN2-depleted cell lines were generated by cloning NSUN2-targeting single guide RNA sequences into the pSpCas9(BB)−2A-Puro (PX459) V2.0 plasmid (Addgene plasmid no. 62988; http://n2t.net/addgene:62988). Plasmids were then transfected into HEK293T cells and Puromycin (Meilunbio) was added at a final concentration of 3 μg/ml to enrich the positively transfected cells 24 h after transfection. After 72 h, the cells were collected and used for genotyping by Sanger sequencing. NSUN6-depleted cell lines were generated in the same way. The primers used for genotyping and single guide RNA sequences are listed in Supplemental Table 4.

Cell viability measurements

HEK293T cells were transfected with DRAM plasmid and cultured at 37°C for 24 h. Subsequently, 1000 cells were seeded in 96-well plates.After waiting for the cells to attach to the wall, the cell activity was detected by Cell Counting Kit-8 (Meilunbio). Cell Counting Kit-8 contains WST-8, which in the presence of the electronically coupled reagent 1-Methoxy PMS can be reduced by mitochondrial dehydrogenase to the orange-colored metazan product Formazan, the absorbance of which is measured at 450 nm to analyze cellular activity.

Western blotting

For protein blotting, samples were lysed in RIPA Lysis Buffer (Meilunbio) with Phenylmethanesulfonyl fluoride (PMSF) and the BCA protein assay kit (Beyotime Biotechnology)

was used to Protein concentration was measured. Total protein extracts were separated by SDS-PAGE on a 10% gel and then transferred to 0.22 nm polyvinylidene fluoride membranes (Boster). Subsequently, the proteins were probed with specific antibodies after the blot was blocked with 5% non-fat milk (Boster). Images were quantified using ImageJ software and all data are expressed as mean ± SEM.

The following antibodies and concentrations were used: NSUN2 Polyclonal antibody (Proteintech; Cat No.20854-1-AP; 1:7500), NSUN6 Polyclonal antibody (Proteintech; Cat No. 17240-1-AP; 1:2000), RabbitAnti-GAPDH antibody (Bioss; bs-41373R; 1:2000), Alpha Tubulin Polyclonal antibody (Proteintech; Cat No. 11224-1-AP; 1:2000), HRP-labeled Goat Anti-Rabbit IgG(H+L) (Beyotime Biotechnology; A0208; 1:2000).

cDNA synthesis and Sanger sequencing

Total cellular RNA was extracted with TRIzol reagent (TIANGEN Biotech) and cDNA was synthesized using PrimeScript™ II 1st Strand cDNA Synthesis Kit (Takara Bio) according to the manufacturer's recommendations. PCR was then performed using 2×Taq PCR MasterMix II (TIANGEN Biotech) and primers flanking m^5C target sites, and the purified PCR products were directly sequenced by Sanger sequencing. The Sanger sequencing results were analyzed using EditR 1.0.10 to calculate the mutation frequency[65]. The primers used in this study are shown in Supplemental Table 4.

Real-time quantitative PCR

cDNA was synthesized using FastKing RT kit (with gDNase) (TIANGEN Biotech) according to the manufacturer's recommendations. RT-qPCR assay was performed using SuperReal PreMix Plus (SYBR Green) (TIANGEN Biotech). GAPDH was used as an endogenous control, and the expression levels were normalized to the control and calculated by the $2^{-\Delta\Delta Ct}$ formula. All samples were analyzed in triplicate and each mRNA quantification represents the average of at least three measurements. All data are expressed as mean ± SEM. The primers used in this study are shown in Supplemental Table 4.

Protein structure modelling

Protein structure simulations were performed using the SWISS-MODEL online website (https://swissmodel.expasy.org/interactive)[66]. The SWISS-MODEL database is able to provide up-to-date annotated 3D protein models, which are generated from automated homology modelling of related model organisms and experimental structural information for all sequences in UniProtKB, with reliable structural information, and subsequently protein structure observations were performed using PyMOL[67].

Bisulfite sequencing PCR

We referenced bisulfite sequencing PCR, an assay established by Matthias Schaefer et al. We chemically deaminated cytosine in RNA using the EZ RNA methylation kit (50) (ZYMO RESEARCH) and then quantified m^5C methylation levels based on PCR amplification of cDNA combined with deep sequencing[23].

RNA Conversion Reagent was premixed with prepared RNA samples, and the RNA was denatured at 70°C for 5 minutes, followed by a reaction period of 45 minutes at 54°C. Finally, the purified RNA samples were recovered after desulfurization by RNA Desulphonation Buffe. cDNA was synthesized using PrimeScript™ II 1st Strand cDNA Synthesis Kit (Takara Bio) according to the manufacturer's recommendations. PCR was then performed using 2× EpiArt HS Taq Master

Mix (Dye Plus) (Vazyme) and m^5C target site specific Bisulfite Primer (primer sequences were designed at https://zymoresearch.eu/pages/bisulfite-primer- seeker), the products were purified by TIANgel Midi Purification Kit (TIANGEN Biotech), and the connectors for second-generation sequencing were attached at both ends of the products for sequencing. Finally, deep sequencing was performed by HiTOM analysis to detect the methylation level (The number of reads >1000 in deep sequencing) [68]. The primers used in this study are shown in Supplemental Table 4.

Library construction and next-generation sequencing

1μl of total cellular RNA was used for sequencing library generation by NEBNext Ultra RNA Library Prep Kit for Illumina (NEB, USA, Catalog #: E7530L) following manufacturer's recommendations and index codes were added to attribute sequences to each sample. Briefly, mRNA was purified from total RNA using poly-T oligo-attached magnetic beads. Fragmentation was carried out using divalent cations under elevated temperature in NEB Next First Strand Synthesis Reaction Buffer(5X). First strand cDNA was synthesized using random hexamer primer and M-MuLV Reverse Transcriptase (RNase H). Second strand cDNA synthesis was subsequently performed using DNA Polymerase I and RNase H. Remaining overhangs were converted into blunt ends via exonuclease/polymerase activities. After adenylation of 3' ends of DNA fragments, NEB Next Adaptor with hairpin loop structure were ligated to prepare for hybridization. To select cDNA fragments of preferentially 370~420 bp in length, the library fragments were purified with AMPure XP system (Beverly, USA). Then 3 μL USER Enzyme (NEB, USA) was used with size selected, adaptor-ligated cDNA at 37°C for 15 min followed by 5 min at 95 °C before PCR. Then PCR was performed with Phusion High-Fidelity DNA polymerase, Universal PCR primers and Index (X) Primer. At last, PCR products were purified (AMPure XP system) and library quality was assessed on the Agilent 5400 system（Agilent ,USA）and quantified by QPCR (1.5 nM). The qualified libraries were pooled and sequenced on Illumina platforms with PE150 strategy in Novogene Bioinformatics Technology Co., Ltd (Beijing, China), according to effective library concentration and data amount required.

DRAM-seq analysis and calling of edited cites

The raw fastq sequencing data were cleaned by trimming the adapter sequences using Fastp (v0.23.1) and were aligned to the human genome (hg19) using STAR (v2.7.7) in paired-end mode. The aligned BAM files were sorted and PCR duplicates were removed using Samtools (v1.12). The cite calling pf DRAM-seq was performed using Bullseye, a previously customized pipeline to look for C-to-U or A-to-G edited sites throughout the transcriptome[40]. Briefly, the sorted and deduplicated BAM files were initially parsed by parseBAM.pl script. Then, Find_edit_site.pl script was employed to find C-to-U or A-to-G editing events by DRAM-seq with at least 10 reads of coverage, an edit ratio of 5%-95%, an edit ratio at least 1.5-fold higher than NSUN2 or NSUN6-knockout samples, and at least 2 editing events at a given site. Sites that were only found in one or two replicates of each DRAM protein variant were removed. Editing events appeared in cells expressing merely APOBEC1 or TadA8e were also removed.

Metagene and motif analyses

Metagene analysis was performed using hg19 annotations according to previously reported tool, MetaplotR[69]. For motif analysis, the 20bp flanking sequence of each DRAM-seq editing site were extracted by Bedtools (v2.30.0)[70]. The motif logos were then plotted by WebLogo (v3.7.12)[71].

Replicates analysis

Independent biological replicates of DRAM-ABE or DRAM-CBE in DRAM-seq analysis were separately compared by computing the Pearson correlation coefficient between the number of C-to-U mutations per mRNA between any two replicate experiments.

GO and KEGG analysis

GO and KEGG analysis of DRAM-seq edited mRNAs was performed using the DAVID bioinformatic database [72]. GO terms with P value of less than 0.05 were considered as statistically significant.

Statistical analysis

All data are expressed as mean ± S.E.M of three independent determinations. Data were analyzed through a two-tailed t-test. A probability of $P < 0.05$ was considered statistically significant; ∗, $P < 0.05$, ∗∗, $P < 0.01$, *, $P < 0.05$, **, $P <0.01$, ***, $P < 0.001$ and ****, $P < 0.0001$ denote the significance thresholds; ns denotes not significant.

Data and Materials Availability

The data supporting the findings of this study are available within the article and its Supplementary Information. Other data and reagents are available from the corresponding authors upon reasonable request.

AUTHOR CONTRIBUTIONS

Conceptualization: JZ, YH, LL, ZL
Methodology: JZ, DZ, JL
Investigation: JZ, DZ, JL, DK, XL, RZ, YL
Visualization: XG, YQ, DW, JC
Supervision: DK, XL, RZ, YL, XG, YQ, DW, JC, YH
Funding acquisition: YH, LL, ZL
Data curation: JZ, YH
Writing—original draft: JZ, DZ, JL
Writing—review & editing: JZ, YH, LL, ZL

Competing Interests

All other authors declare they have no competing interests.

ACKNOWLEDGEMENTS

We thank Yuning Song, Tingting Sui and Yuanyuan Xu for helpful feedback on the project.

FUNDING

This work was supported by the National Natural Science Foundation of China (Nos.32200466).

REFERENCES

1 Wiener, D. & Schwartz, S. The epitranscriptome beyond m(6)A. *Nat Rev Genet* **22**, 119-131 (2021). https://doi.org:10.1038/s41576-020-00295-8

2 Li, S. & Mason, C. E. The pivotal regulatory landscape of RNA modifications. *Annu Rev Genomics Hum Genet* **15**, 127-150 (2014). https://doi.org:10.1146/annurev-genom-090413-025405

3 Van Haute, L. *et al.* NSUN2 introduces 5-methylcytosines in mammalian mitochondrial tRNAs. *Nucleic Acids Res* **47**, 8720-8733 (2019). https://doi.org:10.1093/nar/gkz559

4 Blaze, J. *et al.* Neuronal Nsun2 deficiency produces tRNA epitranscriptomic alterations and proteomic shifts impacting synaptic signaling and behavior. *Nat Commun* **12**, 4913 (2021). https://doi.org:10.1038/s41467-021-24969-x

5 Yang, X. *et al.* 5-methylcytosine promotes mRNA export - NSUN2 as the methyltransferase and ALYREF as an m(5)C reader. *Cell Res* **27**, 606-625 (2017). https://doi.org:10.1038/cr.2017.55

6 Sharma, S., Yang, J., Watzinger, P., Kötter, P. & Entian, K. D. Yeast Nop2 and Rcm1 methylate C2870 and C2278 of the 25S rRNA, respectively. *Nucleic Acids Res* **41**, 9062-9076 (2013). https://doi.org:10.1093/nar/gkt679

7 Hussain, S. *et al.* NSun2-mediated cytosine-5 methylation of vault noncoding RNA determines its processing into regulatory small RNAs. *Cell Rep* **4**, 255-261 (2013). https://doi.org:10.1016/j.celrep.2013.06.029

8 Aguilo, F. *et al.* Deposition of 5-Methylcytosine on Enhancer RNAs Enables the Coactivator Function of PGC-1α. *Cell Rep* **14**, 479-492 (2016). https://doi.org:10.1016/j.celrep.2015.12.043

9 Yang, Y. *et al.* RNA 5-Methylcytosine Facilitates the Maternal-to-Zygotic Transition by Preventing Maternal mRNA Decay. *Mol Cell* **75**, 1188-1202.e1111 (2019). https://doi.org:10.1016/j.molcel.2019.06.033

10 García-Vílchez, R., Sevilla, A. & Blanco, S. Post-transcriptional regulation by cytosine-5 methylation of RNA. *Biochim Biophys Acta Gene Regul Mech* **1862**, 240-252 (2019). https://doi.org:10.1016/j.bbagrm.2018.12.003

11 Trixl, L. & Lusser, A. The dynamic RNA modification 5-methylcytosine and its emerging role as an epitranscriptomic mark. *Wiley Interdiscip Rev RNA* **10**, e1510 (2019). https://doi.org:10.1002/wrna.1510

12 Boo, S. H. & Kim, Y. K. The emerging role of RNA modifications in the regulation of mRNA stability. *Exp Mol Med* **52**, 400-408 (2020). https://doi.org:10.1038/s12276-020-0407-z

13 Courtney, D. G. *et al.* Epitranscriptomic Addition of m(5)C to HIV-1 Transcripts Regulates Viral Gene Expression. *Cell Host Microbe* **26**, 217-227.e216 (2019). https://doi.org:10.1016/j.chom.2019.07.005

14 Liu, J. *et al.* Developmental mRNA m(5)C landscape and regulatory innovations of

massive m(5)C modification of maternal mRNAs in animals. *Nat Commun* **13**, 2484 (2022). https://doi.org:10.1038/s41467-022-30210-0

15 Chen, P., Zhang, T., Yuan, Z., Shen, B. & Chen, L. Expression of the RNA methyltransferase Nsun5 is essential for developing cerebral cortex. *Mol Brain* **12**, 74 (2019). https://doi.org:10.1186/s13041-019-0496-6

16 Flores, J. V. *et al.* Cytosine-5 RNA Methylation Regulates Neural Stem Cell Differentiation and Motility. *Stem Cell Reports* **8**, 112-124 (2017). https://doi.org:10.1016/j.stemcr.2016.11.014

17 Chen, S. Y. *et al.* RNA bisulfite sequencing reveals NSUN2-mediated suppression of epithelial differentiation in pancreatic cancer. *Oncogene* **41**, 3162-3176 (2022). https://doi.org:10.1038/s41388-022-02325-7

18 Chen, X. *et al.* 5-methylcytosine promotes pathogenesis of bladder cancer through stabilizing mRNAs. *Nat Cell Biol* **21**, 978-990 (2019). https://doi.org:10.1038/s41556-019-0361-y

19 Yang, R. *et al.* The RNA methyltransferase NSUN6 suppresses pancreatic cancer development by regulating cell proliferation. *EBioMedicine* **63**, 103195 (2021). https://doi.org:10.1016/j.ebiom.2020.103195

20 Li, Y. *et al.* Long noncoding RNA DIAPH2-AS1 promotes neural invasion of gastric cancer via stabilizing NSUN2 to enhance the m5C modification of NTN1. *Cell Death Dis* **14**, 260 (2023). https://doi.org:10.1038/s41419-023-05781-5

21 Huang, T., Chen, W., Liu, J., Gu, N. & Zhang, R. Genome-wide identification of mRNA 5-methylcytosine in mammals. *Nat Struct Mol Biol* **26**, 380-388 (2019). https://doi.org:10.1038/s41594-019-0218-x

22 Trixl, L., Rieder, D., Amort, T. & Lusser, A. Bisulfite Sequencing of RNA for Transcriptome-Wide Detection of 5-Methylcytosine. *Methods Mol Biol* **1870**, 1-21 (2019). https://doi.org:10.1007/978-1-4939-8808-2_1

23 Schaefer, M., Pollex, T., Hanna, K. & Lyko, F. RNA cytosine methylation analysis by bisulfite sequencing. *Nucleic Acids Res* **37**, e12 (2009). https://doi.org:10.1093/nar/gkn954

24 Amort, T. & Lusser, A. Detection of 5-Methylcytosine in Specific Poly(A) RNAs by Bisulfite Sequencing. *Methods Mol Biol* **1562**, 107-121 (2017). https://doi.org:10.1007/978-1-4939-6807-7_8

25 Cui, X. *et al.* 5-Methylcytosine RNA Methylation in Arabidopsis Thaliana. *Mol Plant* **10**, 1387-1399 (2017). https://doi.org:10.1016/j.molp.2017.09.013

26 Edelheit, S., Schwartz, S., Mumbach, M. R., Wurtzel, O. & Sorek, R. Transcriptome-wide mapping of 5-methylcytidine RNA modifications in bacteria, archaea, and yeast reveals m5C within archaeal mRNAs. *PLoS Genet* **9**, e1003602 (2013). https://doi.org:10.1371/journal.pgen.1003602

27 Saplaoura, E., Perrera, V., Colot, V. & Kragler, F. Methylated RNA Immunoprecipitation Assay to Study m5C Modification in Arabidopsis. *J Vis Exp* (2020). https://doi.org:10.3791/61231

28 Khoddami, V. & Cairns, B. R. Identification of direct targets and modified bases of RNA cytosine methyltransferases. *Nat Biotechnol* **31**, 458-464 (2013). https://doi.org:10.1038/nbt.2566

29 Yuan, F. *et al.* Bisulfite-free and base-resolution analysis of 5-methylcytidine and 5-hydroxymethylcytidine in RNA with peroxotungstate. *Chem Commun (Camb)* **55**, 2328-2331 (2019). https://doi.org:10.1039/c9cc00274j

30 Hayashi, G. *et al.* Base-Resolution Analysis of 5-Hydroxymethylcytosine by One-Pot Bisulfite-Free Chemical Conversion with Peroxotungstate. *J Am Chem Soc* **138**, 14178-14181 (2016). https://doi.org:10.1021/jacs.6b06428

31 Harel, N., Meir, M., Gophna, U. & Stern, A. Direct sequencing of RNA with MinION Nanopore: detecting mutations based on associations. *Nucleic Acids Res* **47**, e148 (2019). https://doi.org:10.1093/nar/gkz907

32 Chang, J. J. *et al.* Transcriptional and epi-transcriptional dynamics of SARS-CoV-2 during cellular infection. *Cell Rep* **35**, 109108 (2021). https://doi.org:10.1016/j.celrep.2021.109108

33 Wan, Y. K., Hendra, C., Pratanwanich, P. N. & Göke, J. Beyond sequencing: machine learning algorithms extract biology hidden in Nanopore signal data. *Trends Genet* **38**, 246-257 (2022). https://doi.org:10.1016/j.tig.2021.09.001

34 Budzko, L., Hoffa-Sobiech, K., Jackowiak, P. & Figlerowicz, M. Engineered deaminases as a key component of DNA and RNA editing tools. *Mol Ther Nucleic Acids* **34**, 102062 (2023). https://doi.org:10.1016/j.omtn.2023.102062

35 Rosenberg, B. R., Hamilton, C. E., Mwangi, M. M., Dewell, S. & Papavasiliou, F. N. Transcriptome-wide sequencing reveals numerous APOBEC1 mRNA-editing targets in transcript 3' UTRs. *Nat Struct Mol Biol* **18**, 230-236 (2011). https://doi.org:10.1038/nsmb.1975

36 Qian, X. *et al.* Low expression of the apolipoprotein B mRNA-editing transgene in mice reduces LDL levels but does not cause liver dysplasia or tumors. *Arterioscler Thromb Vasc Biol* **18**, 1013-1020 (1998). https://doi.org:10.1161/01.atv.18.6.1013

37 Siriwardena, S. U., Chen, K. & Bhagwat, A. S. Functions and Malfunctions of Mammalian DNA-Cytosine Deaminases. *Chem Rev* **116**, 12688-12710 (2016). https://doi.org:10.1021/acs.chemrev.6b00296

38 Richter, M. F. *et al.* Phage-assisted evolution of an adenine base editor with improved Cas domain compatibility and activity. *Nat Biotechnol* **38**, 883-891 (2020). https://doi.org:10.1038/s41587-020-0453-z

39 Gaudelli, N. M. *et al.* Directed evolution of adenine base editors with increased activity and therapeutic application. *Nat Biotechnol* **38**, 892-900 (2020). https://doi.org:10.1038/s41587-020-0491-6

40 Meyer, K. D. DART-seq: an antibody-free method for global m(6)A detection. *Nat Methods* **16**, 1275-1280 (2019). https://doi.org:10.1038/s41592-019-0570-0

41 Sun, Z. *et al.* Effects of NSUN2 deficiency on the mRNA 5-methylcytosine modification and gene expression profile in HEK293 cells. *Epigenomics* **11**, 439-453 (2019). https://doi.org:10.2217/epi-2018-0169

42 Zhang, Q., Zheng, Q., Yu, X., He, Y. & Guo, W. Overview of distinct 5-methylcytosine profiles of messenger RNA in human hepatocellular carcinoma and paired adjacent non-tumor tissues. *J Transl Med* **18**, 245 (2020). https://doi.org:10.1186/s12967-020-02417-6

43 Zhang, Q. *et al.* The role of RNA m(5)C modification in cancer metastasis. *Int J Biol*

Sci **17**, 3369-3380 (2021). https://doi.org:10.7150/ijbs.61439

44 Liu, J. *et al.* Sequence- and structure-selective mRNA m(5)C methylation by NSUN6 in animals. *Natl Sci Rev* **8**, nwaa273 (2021). https://doi.org:10.1093/nsr/nwaa273

45 Schumann, U. *et al.* Multiple links between 5-methylcytosine content of mRNA and translation. *BMC Biol* **18**, 40 (2020). https://doi.org:10.1186/s12915-020-00769-5

46 Fang, L. *et al.* CIGAR-seq, a CRISPR/Cas-based method for unbiased screening of novel mRNA modification regulators. *Mol Syst Biol* **16**, e10025 (2020). https://doi.org:10.15252/msb.202010025

47 Tang, Y. *et al.* OsNSUN2-Mediated 5-Methylcytosine mRNA Modification Enhances Rice Adaptation to High Temperature. *Dev Cell* **53**, 272-286.e277 (2020). https://doi.org:10.1016/j.devcel.2020.03.009

48 Squires, J. E. *et al.* Widespread occurrence of 5-methylcytosine in human coding and non-coding RNA. *Nucleic Acids Res* **40**, 5023-5033 (2012). https://doi.org:10.1093/nar/gks144

49 Zhang, P., Wang, Y. & Gu, X. RNA 5-Methylcytosine Controls Plant Development and Environmental Adaptation. *Trends Plant Sci* **25**, 954-958 (2020). https://doi.org:10.1016/j.tplants.2020.07.004

50 Fletcher, K. *et al.* The WD40 domain of ATG16L1 is required for its non-canonical role in lipidation of LC3 at single membranes. *EMBO J* **37** (2018). https://doi.org:10.15252/embj.201797840

51 Guo, X. *et al.* A Rac/Cdc42-specific exchange factor, GEFT, induces cell proliferation, transformation, and migration. *J Biol Chem* **278**, 13207-13215 (2003). https://doi.org:10.1074/jbc.M208896200

52 Naim, V. & Rosselli, F. The FANC pathway and BLM collaborate during mitosis to prevent micro-nucleation and chromosome abnormalities. *Nat Cell Biol* **11**, 761-768 (2009). https://doi.org:10.1038/ncb1883

53 Anger, A. M. *et al.* Structures of the human and Drosophila 80S ribosome. *Nature* **497**, 80-85 (2013). https://doi.org:10.1038/nature12104

54 Liang, X. *et al.* Structural snapshots of human pre-60S ribosomal particles before and after nuclear export. *Nat Commun* **11**, 3542 (2020). https://doi.org:10.1038/s41467-020-17237-x

55 Gkatza, N. A. *et al.* Cytosine-5 RNA methylation links protein synthesis to cell metabolism. *PLoS Biol* **17**, e3000297 (2019). https://doi.org:10.1371/journal.pbio.3000297

56 Ye, F. *et al.* SIRT1/PGC-1α is involved in arsenic-induced male reproductive damage through mitochondrial dysfunction, which is blocked by the antioxidative effect of zinc. *Environ Pollut* **320**, 121084 (2023). https://doi.org:10.1016/j.envpol.2023.121084

57 McCollum, G., Keng, P. C., States, J. C. & McCabe, M. J., Jr. Arsenite delays progression through each cell cycle phase and induces apoptosis following G2/M arrest in U937 myeloid leukemia cells. *J Pharmacol Exp Ther* **313**, 877-887 (2005). https://doi.org:10.1124/jpet.104.080713

58 Ran, S. *et al.* NaAsO(2) decreases GSH synthesis by inhibiting GCLC and induces apoptosis through Hela cell mitochondrial damage, mediating the activation of the NF-κB/miR-21 signaling pathway. *Ecotoxicol Environ Saf* **234**, 113380 (2022).

https://doi.org:10.1016/j.ecoenv.2022.113380

59 Schaefer, M. RNA 5-Methylcytosine Analysis by Bisulfite Sequencing. *Methods Enzymol* **560**, 297-329 (2015). https://doi.org:10.1016/bs.mie.2015.03.007

60 Bourgeois, G. *et al.* Eukaryotic rRNA Modification by Yeast 5-Methylcytosine-Methyltransferases and Human Proliferation-Associated Antigen p120. *PLoS ONE* **10**, e0133321 (2015). https://doi.org:10.1371/journal.pone.0133321

61 Gu, X. & Liang, Z. Transcriptome-Wide Mapping 5-Methylcytosine by m(5)C RNA Immunoprecipitation Followed by Deep Sequencing in Plant. *Methods Mol Biol* **1933**, 389-394 (2019). https://doi.org:10.1007/978-1-4939-9045-0_24

62 Kim, K., Shi, A. B., Kelley, K. & Chen, X. S. Unraveling the Enzyme-Substrate Properties for APOBEC3A-Mediated RNA Editing. *J Mol Biol* **435**, 168198 (2023). https://doi.org:10.1016/j.jmb.2023.168198

63 Barka, A. *et al.* The Base-Editing Enzyme APOBEC3A Catalyzes Cytosine Deamination in RNA with Low Proficiency and High Selectivity. *ACS Chem Biol* **17**, 629-636 (2022). https://doi.org:10.1021/acschembio.1c00919

64 Pan, Y. *et al.* Nanoscale Characterization of Interaction of APOBEC3G with RNA. *Biochemistry* **56**, 1473-1481 (2017). https://doi.org:10.1021/acs.biochem.6b01189

65 Kluesner, M. G. *et al.* EditR: A Method to Quantify Base Editing from Sanger Sequencing. *Crispr j* **1**, 239-250 (2018). https://doi.org:10.1089/crispr.2018.0014

66 Bienert, S. *et al.* The SWISS-MODEL Repository-new features and functionality. *Nucleic Acids Res* **45**, D313-d319 (2017). https://doi.org:10.1093/nar/gkw1132

67 Delano, W. L. The PyMol Molecular Graphics System. *Proteins Structure Function and Bioinformatics* **30**, 442-454 (2002).

68 Liu, Q. *et al.* Hi-TOM: a platform for high-throughput tracking of mutations induced by CRISPR/Cas systems. *Sci China Life Sci* **62**, 1-7 (2019). https://doi.org:10.1007/s11427-018-9402-9

69 Olarerin-George, A. O. & Jaffrey, S. R. MetaPlotR: a Perl/R pipeline for plotting metagenes of nucleotide modifications and other transcriptomic sites. *Bioinformatics* **33**, 1563-1564 (2017). https://doi.org:10.1093/bioinformatics/btx002

70 Quinlan, A. R. & Hall, I. M. BEDTools: a flexible suite of utilities for comparing genomic features. *Bioinformatics* **26**, 841-842 (2010). https://doi.org:10.1093/bioinformatics/btq033

71 Crooks, G. E., Hon, G., Chandonia, J. M. & Brenner, S. E. WebLogo: a sequence logo generator. *Genome Res* **14**, 1188-1190 (2004). https://doi.org:10.1101/gr.849004

72 Sherman, B. T. *et al.* DAVID: a web server for functional enrichment analysis and functional annotation of gene lists (2021 update). *Nucleic Acids Res* **50**, W216-w221 (2022). https://doi.org:10.1093/nar/gkac194

FIGURES LEGENDS

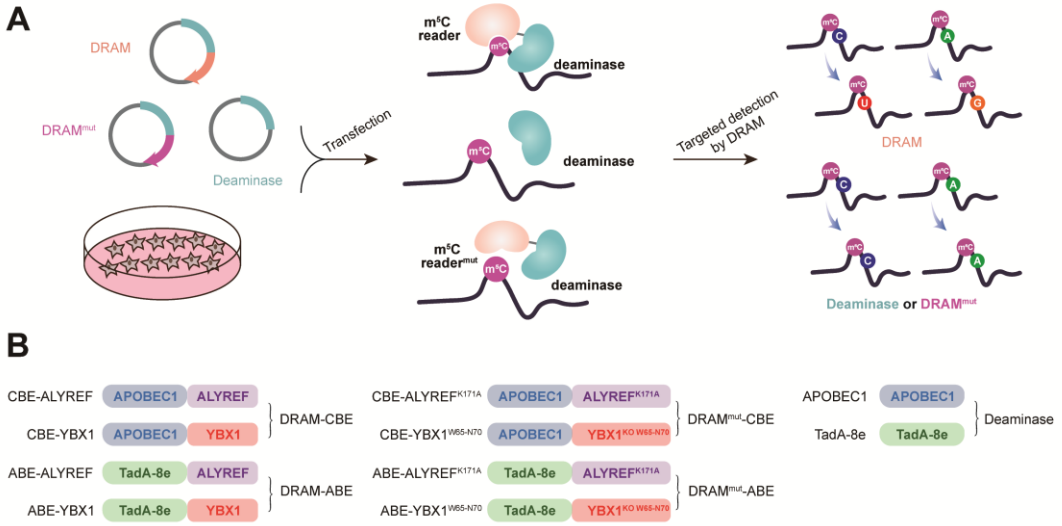

Fig.1: **Development of DRAM system for m^{5}C detection.**

(A) Schematic diagram of the DRAM assay. DRAM, DRAM^{mut} and Deaminase system were transfected into HEK293T cells separately. After DRAM transfection, the deaminase was directed by m^{5}C reader to the vicinity of the m^{5}C site and induce C-to-U/A-to-G mutations, whereas transfection of the DRAM^{mut} or Deaminase system failed to effectively induce similar mutations due to the absence of the m^{5}C-recognition-binding domain.

(B) The overall design of DRAM, DRAM^{mut} and Deaminase system.

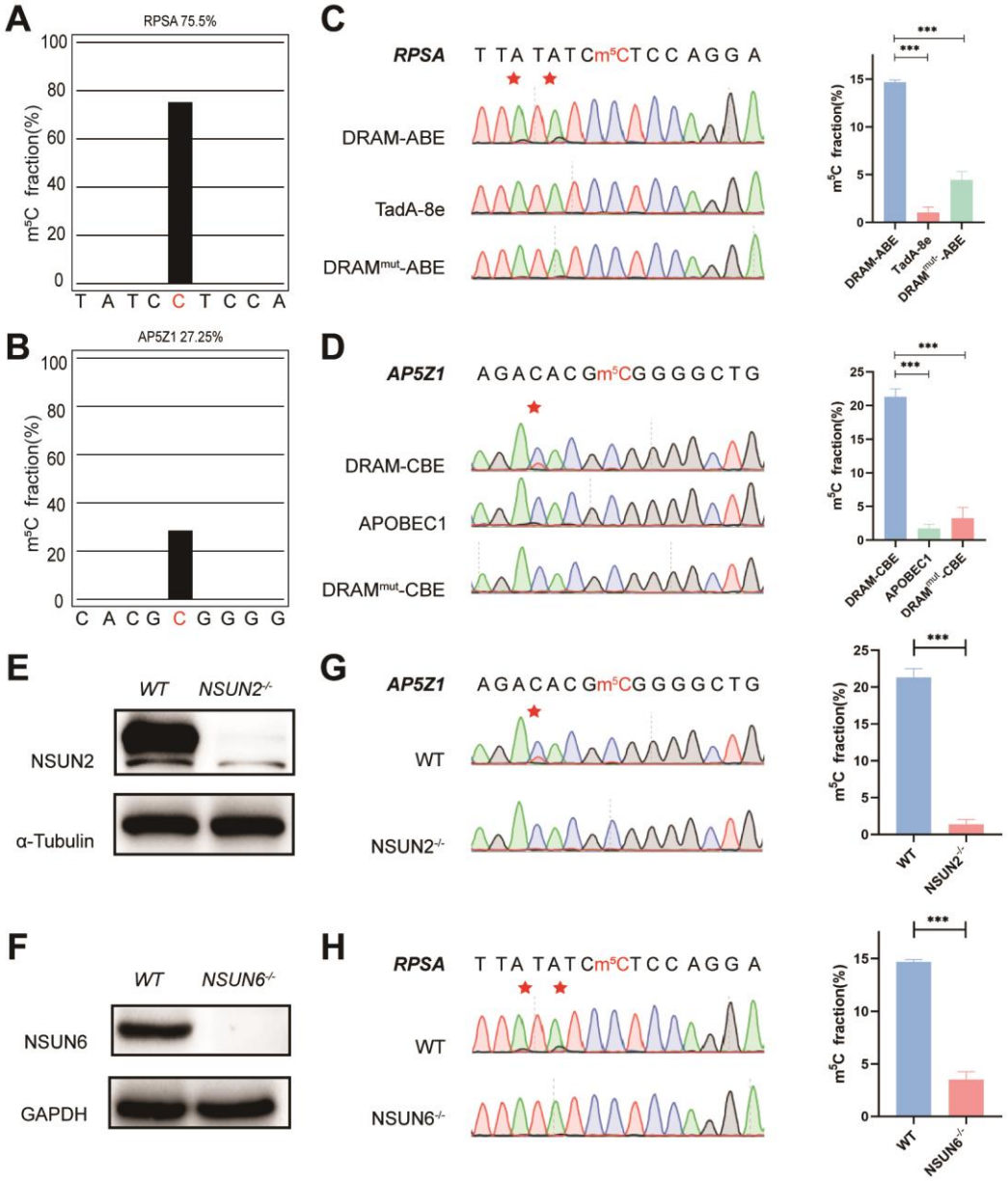

Fig.2: DRAM detection system was assayed in an m^{5}C -dependent form.

(A, B) Two m^{5}C sites from RPSA (**A**) and AP5Z1 (**B**) mRNA detected by deep sequencing of bisulfite sequencing PCR in HEK293T cells. The m^{5}C sites are highlighted by red color. The deamination rates of RPSA and AP5Z1 were 75.5% and 27.25% (The number of reads is greater than 1000).

(C, D) Sanger sequencing following RT-PCR verified two m^{5}C sites from RPSA (**C**) and AP5Z1 (**D**) mRNAs in DRAM-transfected HEK293T cells, respectively. HEK293T cells only expressing DRAM^{mut} or Deaminase were served as negative controls. The left panel illustrates the location of DRAM induced mutation sites, which is highlighted in red asterisk. The right panel shows the corresponding quantification of sanger sequencing.

(E, F) The knockout efficiency of NSUN2 (**E**) and NSUN6 (**F**) in HEK293T cell lines verified by Western blotting. The protein level of α-Tubulin and GAPDH were served as loading controls, separately.

(G, H) DRAM induced mutations close to m^5C sites in AP5Z1 (**G**) and RPSA (**H**) mRNAs after NSUN2 and NSUN6 knockout in HEK293T cells. The left panel illustrates the location of DRAM induced mutation sites, which is highlighted in red asterisk. The right panel shows the corresponding quantification of sanger sequencing.

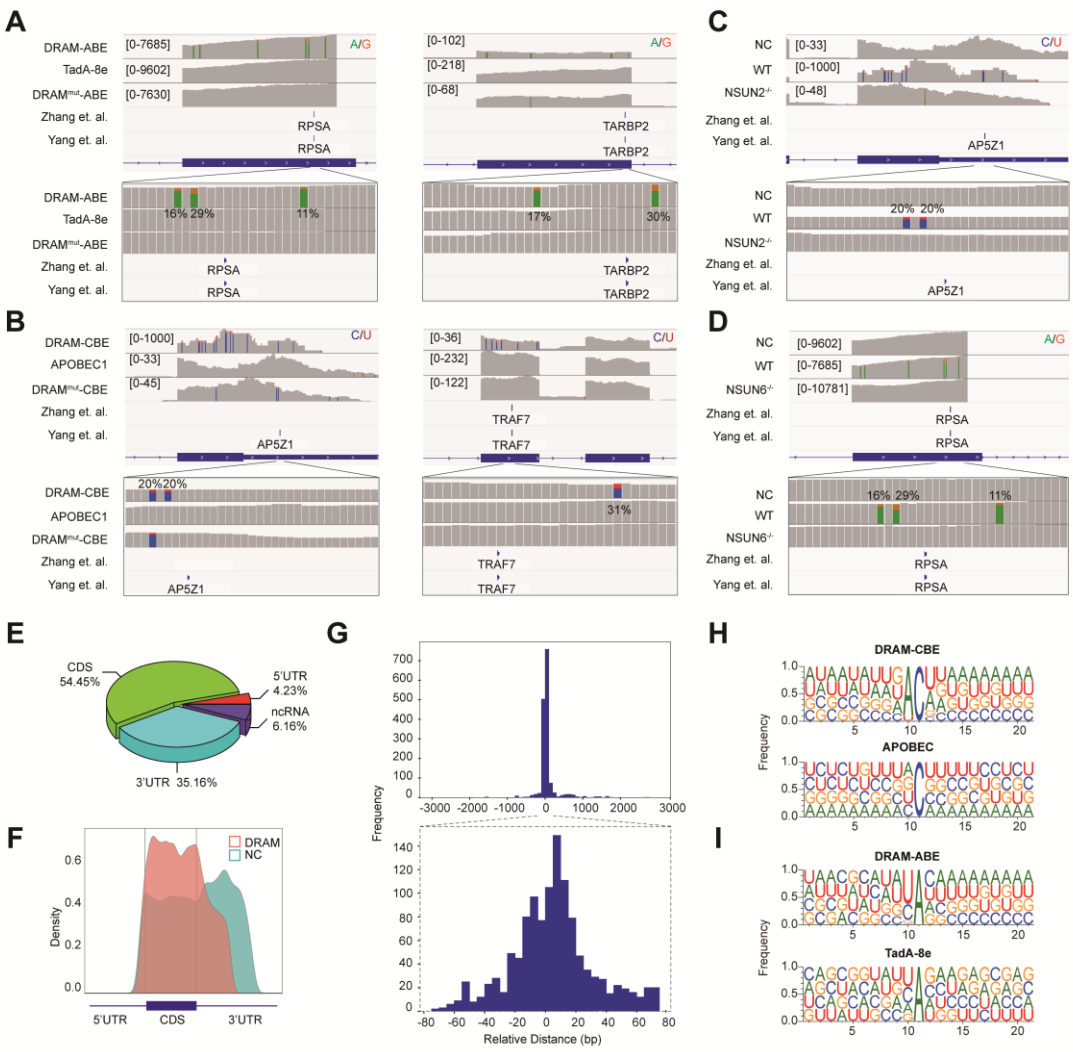

Fig.3: DRAM enables transcriptome-wide analysis of m^{5}C methylation.

(A, B) Integrative genomics viewer (IGV) browser traces of DRAM-seq data expressing the indicated constructs in RPSA (**A**, left panel), TARBP2 (**A**, right panel), AP5Z1(**B**, left panel), and TRAF7 (**B**, left panel) mRNAs. C-to-U or A-to-G mutations found in at least 10% of reads are indicated by coloring. The previously published RNA BS-seq datasets from two individual studies were displayed as panel "Yang et al." and "Zhang et al.". (n(DRAM)=3 independent samples, n(Deaminase)=2 independent samples, and n(DRAM^{mut})=1 independent sample.)

(C, D) Integrative genomics viewer (IGV) browser traces of DRAM-seq data in wildtype and methyltranferases knockout cells in AP5Z1 (**C**) and RPSA (**D**) mRNAs. C-to-U or A-to-G mutations were found in at least 10% of reads are indicated by coloring. The previously published RNA BS-seq datasets from two individual studies were displayed as panel "Yang et al." and "Zhang et al.". n=3 independent samples.

(E) The pie chart shows the distribution of editing sites in different transcript region in cells expressing DRAM (n=3 independent samples).

(F) The density map showing the distribution of editing events across the mRNA transcripts detected by DRAM-seq.

(G) The frequency plot shows the distribution of the distances of edit events in DRAM-seq relative to the m^{5}C sites from the published BS-seq datasets. The position of each m^{5}C site of

BS-seq is
determined as 0, and the relative distance of each site to the nearest edit event in DRAM-seq is calculated and plotted. The plots are presented separately based on the cutoff of upstream and downstream 3000bp (above) and 80bp (below) windows.
(H, I) Motif analysis discovered within the ±20nt region around the C-to-U or A-to-G editing site in cells expressing DRAM-CBE (**H)**, APOBEC1(**H)**, DRAM-ABE (**I)** and TadA-8e (**I)**.

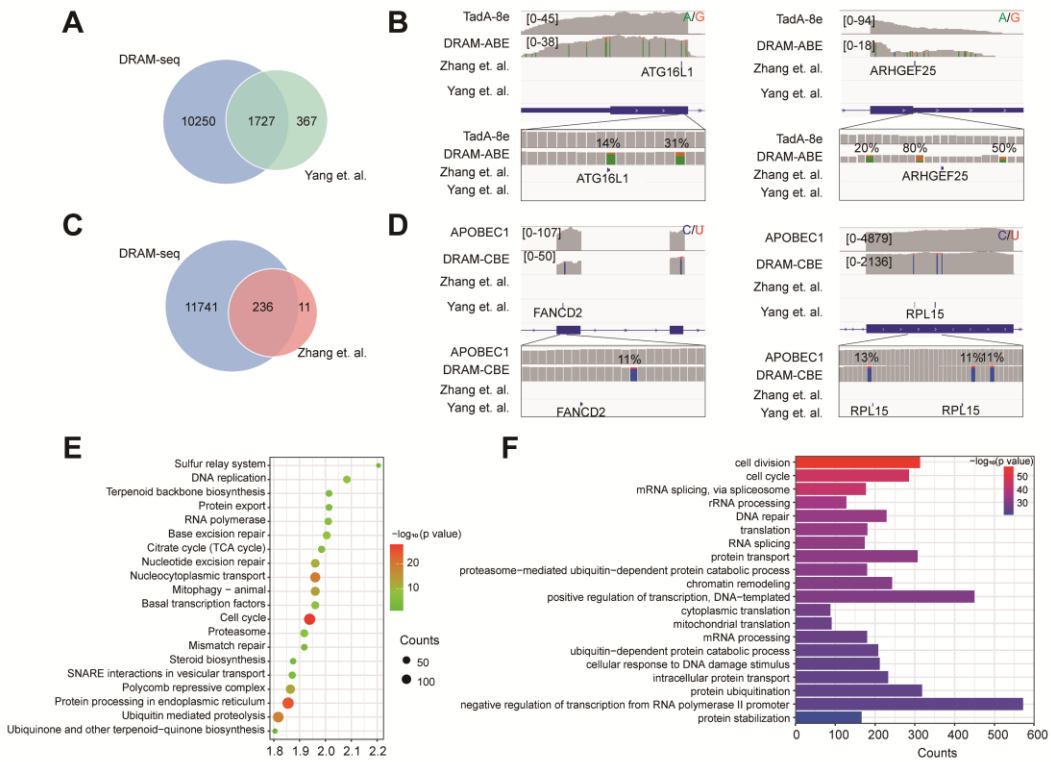

Fig.4: DRAM monitors m^{5}C dynamics in cellular RNA.

(**A**) Venn diagram showing the overlap between DRAM-seq and Yang et al.'s edited genes.

(**C**) Venn diagram showing the overlap between DRAM-seq and Zhang et al.'s edited genes.

(**B**, **D**) Integrative genomics viewer (IGV) browser traces of DRAM-seq data expressing the indicated constructs in the ATG16L1(**B**), ARHGEF25(**B**), FANCD2(**D**), and RPL15(**D**) mRNAs. C-to-U/A-to-G mutations found in at least 10% of reads are indicated by coloring, and the m^{5}C site found by BS-seq is also labelled.

(**E**) Genes with DRAM-seq editing events were analyzed for KEGG bioprocess enrichment.

(**F**) GO biological processes enrichment analysis of genes with DRAM-seq editing events. Statistical analyses were performed using the DAVID tool.

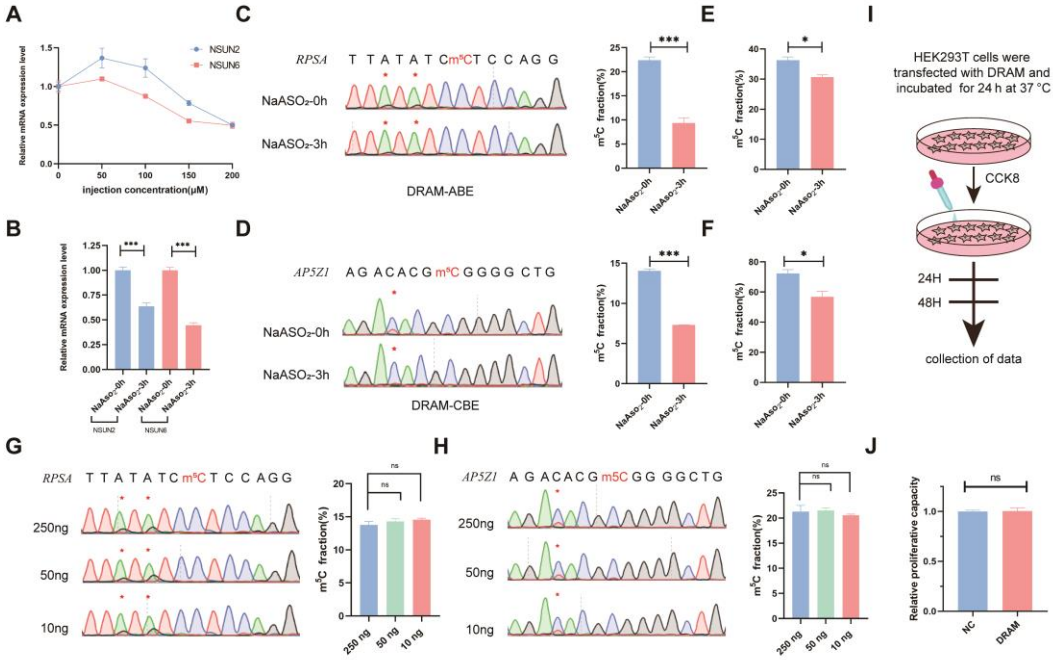

Fig.5: DRAM monitors m^{5}C dynamics in cellular RNA.

(A) Relative expression levels of NSUN2 and NSUN6 mRNA in HEK293T cells treated with 50 μM, 100 μM, 150μM and 200μM $NaAsO_2$.

(B) Relative expression levels of NSUN2 and NSUN6 mRNA in DRAM-expressing HEK293T cells treated with 200μM $NaAsO_2$ for 3 hours.

(C, **D**) The m^{5}C adjacent mutations from RPSA (**C**) and AP5Z1 (**D**) mRNA in DRAM-expressing HEK293T cells treated with $NaAsO_2$. The left panel indicates the sanger sequencing results following RT-PCR, while the corresponding quantifications of DRAM-induced mutations are shown on the right panel.

(E, **F**) BS-PCR showing the m^{5}C levels in RPSA and AP5Z1 mRNAs after 3 h of control and $NaAsO_2$ treatment in cells.

(G, **H**) DRAM analysis of RPSA (**G**) and AP5Z1 (**H**) mRNAs with 250 ng, 50 ng, and 10 ng of input RNA. Representative Sanger sequencing plots are shown on the left panel, with mutation sites marked with asterisks. The mutation rates are quantified on the right panel.

(I) Flowchart illustrating Cell viability analysis by CCK8 reagent after DRAM transfection in HEK293T cells.

(J) Quantitative comparison of the relative proliferative capacity of DRAM-expressing and untransfected cells.